https://doi.org/10.3311/PPci.42813

Periodica Polytechnica Civil Engineering, 70(1), pp. 301–314, 2026

Hydrological Mass Variations in Major River Basins in China with the Use of GRACE Monthly Gravity Field Models

Duan Yang[1*], László Báder[2], Lóránt Földváry[3*]

[1] School of Geomatics and Urban Spatial Informatics, Beijing University of Civil Engineering and Architecture, 15 Yongyuan Road, Daxing District, 102616 Beijing, China
[2] Department of Hydraulic and Water Resources Engineering, Faculty of Civil Engineering, Budapest University of Technology and Economics, Műegyetem rkp. 3., H-1111 Budapest, Hungary
[3] Department of Geodesy and Surveying, Faculty of Civil Engineering, Budapest University of Technology and Economics, Műegyetem rkp. 3., H-1111 Budapest, Hungary
[*] Corresponding author, e-mail: foldvary.lorant@emk.bme.hu

Received: 13 November 2025, Accepted: 14 February 2026, Published online: 20 March 2026

Abstract

Mass redistributions within the Earth system induce changes in the planet's gravity field, observable *via* the Gravity Recovery and Climate Experiment (GRACE) mission. GRACE data have become essential for monitoring large-scale hydrological processes. While GRACE captures water mass variations at the basin scale, *in situ* hydrological stations provide localized insights based on water level and volume changes. This study investigates water mass variations across the major river basins of mainland China, aiming to link basin-scale GRACE observations with local *in situ* measurements. Building on previous findings from the La Plata River basin, this research explores the potential phase lag between GRACE-derived mass changes and tide gauge records. However, no significant phase lag was identified in Chinese basins, likely due to intensive water management practices that also affect subsurface water storage. Nevertheless, the GRACE-derived sur-face mass variations were validated, showing strong temporal and spatial agreement with simulated total water storage anomalies from the CLHMS model and ERA5-Land reanalysis.

Keywords

water mass variation, GRACE monthly solutions, China major river basins, tide gauge observations, total water storage

1 Introduction

The Earth is a dynamic system undergoing constant change [1]. All components of the Earth system – the geosphere (land), atmosphere (air), hydrosphere (water), cryosphere (ice), and biosphere (living organisms) – are subject to processes that alter mass distribution, affecting the Earth's gravitational field across both spatial and temporal scales [2], summarized on Fig. 1 [3].

In the 2000s, satellite gravimetry missions were launched to refine global gravity models and capture temporal mass variations with resolutions of approximately 100 km. The origins of satellite gravimetry date back to the 1950s, with initial measurements of Earth's oblateness taken using the Sputnik satellite in 1958. Subsequent missions, such as LAGEOS I (1976) and LAGEOS II (1992), offered insight into both static and seasonal variations of the gravity field [4]. However, these early satellites had limited capabilities for detecting fine-scale or short-term mass changes.

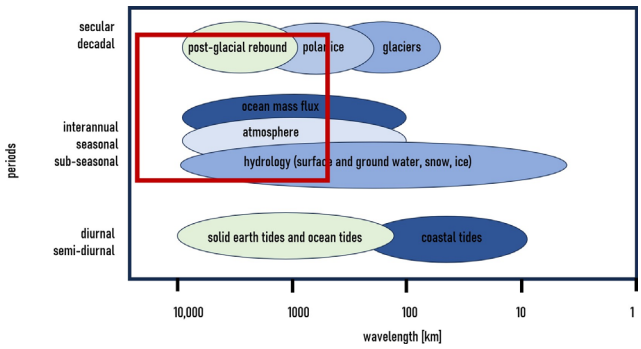

Fig. 1 Geophysical phenomena that drive measurable temporal and spatial variations in the Earth's gravity field (modified from [3])

The 2000s marked a significant advancement in satellite gravimetry. The CHAMP mission, launched in 2000, employed a high-low satellite-to-satellite tracking (SST) system using GPS signals. Orbiting initially at 450 km (later reduced to 250 km), CHAMP operated

Cite this article as: Yang, D., Báder, L., Földváry, L. "Hydrological Mass Variations in Major River Basins in China with the Use of GRACE Monthly Gravity Field Models", Periodica Polytechnica Civil Engineering, 70(1), pp. 301–314, 2026. https://doi.org/10.3311/PPci.42813

until 2010 [5]. GRACE, launched in 2002 and operational until 2017, used a low-low SST configuration with twin satellites separated by 220 ± 50 km, providing monthly global gravity field data with near-uniform coverage [6]. GOCE, operational from 2009 to 2013, introduced satellite gravity gradiometry (SGG), which measured second-order derivatives of Earth's gravitational potential, further improving spatial resolution [7].

The GRACE has provided a unique tool for observing temporal variations of the gravity field, as the monthly homogeneous distribution of measurements enables the determination of monthly gravity field models. Monthly temporal gravity variations are suitable for determination of seasonal mass variations, which are mainly contributed by the annual and semi-annual periods. Relevant mass variations with annual period are observed as a consequence of the illumination by the Sun and the corresponding laws of thermodynamics [1]. Such variations are contributed by the atmosphere (large-scale latitudinal (the Hadley, Ferrel and polar cells) and longitudinal (Walker circulation and El Niño – Southern Oscillation) atmospheric circulations), biosphere (seasonal variations of vegetation on land and phytoplankton on the ocean surface), cryosphere (ice mass balance variations of Antarctica, Greenland and permafrost), hydrosphere (major ocean mass transportation processes of the oceans and hydrological mass variations of the water cycle over continents), and geosphere (solid Earth tide processes, Earth core variations) [8].

The present study is dealing with the determination of hydrological mass variations in major river basins in China with the use of GRACE monthly gravity field models. The methodology of this study was intended to follow the study of Kiss and Földváry [9] but has been changed accordingly to the results. The conclusion of that study is that time delay between GRACE data and tide gauge data has been found to be 11–13 days on the annual period. Furthermore, there were spatially different estimations observed, such as close to the estuary of a river the periods of the different influents and subsurface sources were detected to be so much mixed that relevant annual period could have not been determined. Also, it was found that rivers under heavy water control, i.e., dams and subsurface aquifers, no periodicity of the water mass variations on annual period could be seen neither on GRACE nor on tide gauge water level data. In the present study, similar tendencies were attempted to be determined in this study, and the differences in the observations were discussed subsequently.

Studies by Li et al. [10] and Li and Li [11] analyzed terrestrial water storage anomalies (TWSA) in China for monitoring of regional water resources with daily temporal resolution. Generally, the outcome of these studies is that identifying and accounting for time-correlated noise is essential for accurate hydrological monitoring, furthermore, it was found that traditional methods, i.e., hydrological/gauging stations or groundwater wells, significantly underestimate the uncertainty of water trends. This is a comparable result with the observations for the Amazon region [12] and can be interpreted by basic sampling considerations [13].

2 Major river basins of China

China's major river basins play a central role in the country's hydrological regime. Due to China's diverse topography and climate, the natural hydrological conditions vary widely across basins [14]. Most major rivers traverse vast geographical regions and flow predominantly from west to east, following the general decline in elevation across the country [15].

Rivers in China are typically categorized as either outflowing (draining into the ocean) or inflowing (terminating inland). Outflow rivers account for about 64% of China's land area. This study focuses on five major outflow rivers: the Liao River, Huai River, Yel-low River (Huang He), Yangtze River, and Pearl River (Zhu Jiang) (Fig. 2). Each of these rivers is over 1,000 km long, with drainage areas ranging from 180,000 to 1.8 million km^2.

The Qinling-Huaihe Line serves as a key geographical divide, separating northern and southern river basins with distinct hydrological features. Northern basins, including the Yellow and Liao Rivers, lie in semi-arid or semi-humid zones, experience winter ice cover, and are less influenced by precipitation or seasonal floods. In contrast, southern basins such as the Yangtze and Pearl Rivers flow through humid regions with higher precipitation and denser vegetation [16]. The Huai River straddles this boundary and exhibits transitional characteristics.

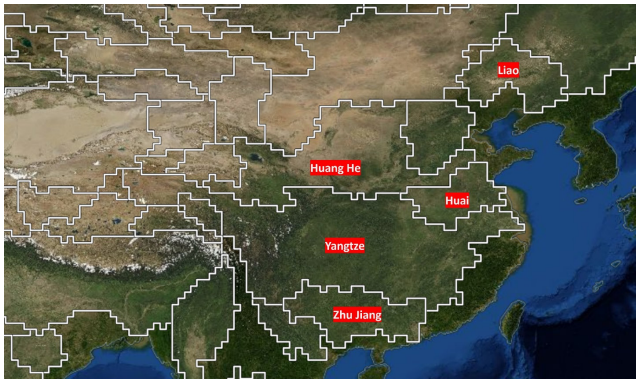

Fig. 2 Major river basins of China used in this study

3 Data

This study utilizes two primary data sources: time series of water levels from in situ gauge measurements and surface mass variations observed by the GRACE satellites. To explore the relationship between these datasets, it is essential that the selected river basins contain sufficient data from both sources.

3.1 GRACE water equivalent thickness

Surface mass anomaly, denoted as $\Delta\sigma$ refers to the mass redistribution occurring at or near Earth's surface. It can be expressed in spherical harmonic expansion as follows [17, 18]:

$$\Delta\sigma(\vartheta,\lambda) = \frac{R\rho_{\text{Earth}}}{3}\sum_{n=0}^{n_{\max}}\frac{2n+1}{1+k_n}\sum_{m=0}^{n}\left[\begin{matrix}\Delta C_{n,m}\cos(m\lambda)\\ +\Delta S_{n,m}\sin(m\lambda)\end{matrix}\right]P_{n,m}\left(\sin(\vartheta)\right), \tag{1}$$

where ϑ is the co-latitude, λ is the longitude, R is the mean radius of the Earth, ρ_{Earth} is the average density of the Earth, $n_{\max}$ is the maximal degree of the spherical expansion, k_n represents the load Love numbers, which describes the response of the Earth crust for surface mass loads; $\Delta C_{n,m}$ and $\Delta S_{n,m}$ are the residual spherical harmonics coefficients of degree n and order m, and $P_{n,m}$ are the Legendre polynomials.

The surface mass anomaly provides insights into mass redistributions within the hydrosphere, measured in kg/m^2. Dividing this by the water density yields the Equivalent Water Height (EWH), a unit of hydrological change in terms of water column height:

$$\frac{\Delta\sigma\left(\left[\frac{\text{kg}}{\text{m}^2}\right]\right)\rightarrow\Delta\sigma\left(\left[\frac{\text{kg}}{\text{m}^2}\right]\right)}{\rho_{\text{water}}\left(\left[\frac{\text{kg}}{\text{dm}^3}\right]\right)} = \text{EWH}\left([\text{mm}]\right), \tag{2}$$

where ρ_{water} is the density of water in kg/dm^3.

GRACE-borne observations of the monthly changes in the gravitational field are caused by mass redistributions, which can be interpreted as anomalies concentrated in a thin layer of water near the Earth's surface. In reality, the majority of these anomalies are caused by changes in the water stored in hydrological reservoirs (catchments), changing oceanic, atmospheric and land ice masses, and mass exchange between these parts of the Earth system. Their amount is measured in centimeters as the height of an equivalent water column (EWH).

Release 06 of all official GRACE / GRACE-FO processing centers (i.e., JPL (Jet Propulsion Laboratory) [19], GFZ (GeoforschungsZentrum Potsdam) [20] and CSR (Center for Space Research at University of Texas, Austin) [19]) were tested, but as no essential differences were observed, only monthly solutions of JPL are presented in this paper. Based on the spherical harmonic coefficients of each monthly gravity field solutions, surface mass anomalies were determined by Eq. (1) in a 1 × 1 degree grid for each basin from April 2002 to October 2023. Surface mass density variations with monthly resolution are dominated by the mass variations of ocean and hydrology over the test area. The area of the basin has been outlined by the method of Longuevergne et al. [21] to reduce mass variation effects of the neighboring regions and of the ocean, thus the remaining signal may be assumed to be generated by hydrological processes within a basin. The catchment basins were delimited according to boundaries by the NASA [22]. Average surface mass variations have been calculated for each basin, and the observed periodic signal has been compared to tide gauge measurements. The maximal degree of the spherical harmonics has been truncated at l = 60. In order to eliminate the striping features of the GRACE monthly solutions, a Gaussian smoothing with radius r = 300 km and a de-striping filter [18] have been applied.

3.2 Hydrological water level

Hydrological data for this study were sourced from the Hydroweb database [23], which provides time series of water levels for rivers and lakes globally, including several in China. The primary goal is to compare local water level changes with the average mass variations observed by GRACE satellites. To ensure that the hydrological data aligns with the basins defined for the GRACE data, only stations within the boundaries of these basins were selected.

The number of virtual stations within each river basin depends on the river's size and can range from dozens to several hundred (see Table 1). Since such a large number of stations is unnecessary for accurately depicting mass anomaly variations at the spatial resolution of the GRACE data, a thinning method was applied. Virtual stations were selected based on even spacing along the river, ensuring that the extracted data would be well-distributed. For regions with multiple stations, the station with the longest available time series was prioritized. The final number of selected stations for each river basin is listed in the 3rd column of Table 1.

Table 1 Number of virtual stations selected from river basins

Basins	Number of all stations	Number of selected stations	Number of reliable stations
Liao River	42	28	21
Huai	37	16	9
Yellow	138	45	17
Yangtze	356	31	22
Pearl	96	17	15
Summary	669	137	84

Time series of water levels were used to establish cross-correlation with the GRACE-derived surface mass anomalies. Methodologically, cross-correlation between the two time series is to be established for detecting the phase shift between the two, which may lead to nonsense results as well, in cases when the curves show less relevant periodic component. In most of the occasions, we considered that if correlation coefficient is less than 0.3, the impact of the hydrological processes is not dominant among other local mass redistribution processes, so such stations are excluded from the analysis. But in some special cases, correlation might be affected by other factors which requires further analyses. The not convincing cases are labelled to be 'unreliable' from the perspective of phase de-termination, and are excluded from the analysis (some examples of the filtered stations are shown in Appendix A). The number of the remaining 'reliable' virtual stations are listed in Table 1.

4 Methodology

4.1 Loess regression

The GRACE-borne surface mass anomaly time series are to be compared with *in situ* gauged water level observations along the major rivers of a certain basin. However, both surface mass anomaly and gauge data show relevant inter-annual fluctuations. When comparison is performed, and correlation of the two curves are to be determined, these fluctuations might notably distort the results. Therefore, a low-pass filtered version of both time series are derived.

Low-pass filtering was performed using the Locally Estimated Scatterplot Smoothing (LOESS) method. LOESS is a nonparametric technique for smoothing data where no assumptions about the underlying structure are made. The method employs local regression to fit a smooth curve through the data.

LOESS is particularly useful when classical methods do not perform well or cannot be applied efficiently. It combines the simplicity of linear least squares regression with the flexibility of nonlinear regression by fitting simple models to localized subsets of data. The model is then used to build a point-by-point function that captures the deterministic variation in the data. One of the key advantages of LOESS is that it does not require a predefined global function to fit the model; it only needs to fit locally to the data segments. However, this increases the computational demand [24].

The LOESS method, proposed by Cleveland [25] and Cleveland and Devlin [26], refers to locally weighted polynomial regression. A low-degree polynomial is fitted to a subset of data at each point, with the degree of the polynomial and the weights being flexible parameters. The weighted least squares approach gives more weight to points close to the target point and less weight to those further away. The fitted polynomial is then evaluated to produce the regression function for each data point.

4.2 Cross-correlation

When (GRACE-borne) surface mass anomaly and (gauged) water level data are compared, we assume a phase occurring between the two time series (c.f., Kiss and Földváry [9]) due to their generally different characteristics. While gauged data shows locally (point-wisely) the variation of the water level, the GRACE-borne data show an integrated mass change, including all mass variations within the basin regardless whether it is above or below the surface. This difference can be interpreted as the GRACE time series is a real average, while the gauge time series is the local change. As it takes for the tides to go down along a river, by approaching to the estuary, an increase in the phase lag between the two time series can be expected. Based on the change of the phase lag, the time required for a tidal wave to recede can be estimated. For determination of the phase lag, cross-correlation of the two time series was determined.

In signal processing, cross-correlation (or cross-covariance) is a measure of the similarity between two signals. The cross-correlation, Γ_{AB} between two signals, A and B is defined (according to the statistical approach) as [27]:

$$\Gamma_{AB}(\tau) = \mathbb{E}\big(A(t)\,B(t-\tau)\big), \tag{3}$$

where $\mathbb{E}$ is the expectation value, while t and τ refer to different time variables. From another point of view, the cross-correlation as the function of the time can be defined as [27]:

$$\Gamma_{AB}(\tau) = A * B^{*}(-) = \int A(t)\,B(t-\tau)\,dt, \tag{4}$$

where the * symbol refers to the convolution, and the * operator is the complex conjugate. The two definitions are equivalent if the signals are ergodic to order two. The Fourier transform of the cross-correlation is the spectral density, γ_{AB}:

$$\gamma_{AB}(\tau) = \mathcal{F}\left(\Gamma_{AB}(\tau)\right) = \mathcal{F}\left(A(t)\right) \times \mathcal{F}\left(B^{*}(-t)\right) = a(\upsilon) \times b^{*}(\upsilon), \tag{5}$$

where $\mathcal{F}$ is the Fourier transform, and υ is the frequency. The convolution product is equivalent to the cross-correlation of $A(t)$ and $B^*(-t)$.

For practical interpretation, let us take two real-valued functions, A and B. Cross-correlation can be used to find how much B must be shifted along the x-axis to be equal to A. The formula is essentially B shifted along the x-axis and calculating the integral of their multiplication at each position. At the phase lag, where the functions are most similar to each other, the A^*B is maximized. This is because if the vertices (positive areas) are in a line, they contribute greatly to the integral. Likewise, when the troughs (negative areas) are in a line, they also contribute positively to the integral because the product of two negative numbers is positive [27].

4.3 Annual variation

Classically, annual variations are determined by Least Square fit of a polynomial consisting of relevant periodic, linear and bias terms, e.g.,:

$$f(t) = a + b \times t + c \times \sin\left(\omega_{\text{annual}} t + \varphi_c\right) + d \times \sin\left(\omega_{\text{semi-annual}} t + \varphi_d\right), \tag{6}$$

where a is the bias, b is the linear trend, c and φ_c are the amplitude and phase of the variations on annual period, ω_{annual}, and d and φ_c are the amplitude and phase of the variations on semi-annual period, $\omega_{\text{semi-annual}}$ of the time series, $f(t)$ [28]. In such a way, however, in case of a temporally smoothed observation (such as the GRACE-borne monthly surface mass variation series) the amplitude of the periodic signal is underestimated, resulting in an underestimation of the involved water mass. This can be resolved by changing the formula as follows [22]:

$$f(t) = a + b \times t + c \times \frac{1}{\operatorname{sinc}\left(\frac{1}{12}\right)} \times \sin\left(\omega_{\text{annual}} t + \varphi_c\right) + d \times \frac{1}{\operatorname{sinc}\left(\frac{1}{6}\right)} \times \sin\left(\omega_{\text{semi-annual}} t + \varphi_d\right). \tag{7}$$

The sinc terms in Eq. (7) are restoring the energy of the periodic signal, resolving the smoothing effect of the temporal averaging of the monthly solutions [13].

5 Results

5.1 Liao River

A total of 28 gauged water level stations were extracted from the Liao River basin. The normalized correlation between the gauged water level and GRACE-derived water equivalent thickness (EWH) time series ranges from 0.1 to 0.8. These results, calculated without any phase shift (hereafter referred to as "correlation"), are summarized in Table 2.

The spatial distributions of correlation coefficients and phase lags are shown in Figs. 3 and 4, respectively. The variation of phase lag along the river as a function of distance from the estuary (in kilometers) is illustrated in Fig. 5.

5.2 Huai River

The Huai River has the fewest gauged water level stations among the five study basins, with a total of 15 selected. The correlation between the full time series without phase shift ranges from 0.02 to 0.73. Reliable station results are summarized in Table 3. Station positions are represented in kilometers from the river estuary ("Reference Distance"

Table 2 Results for reliable stations in Liao River basin

Reference distance (km)	Lag (days)	Normalized correlation	Loess lag (days)	Loess correlation
1215	−176	0.3051	−202	0.0056
1198	233	0.3697	360	0.1656
1187	113	0.5706	161	0.3144
1034	96	0.5032	115	0.1949
1006	−172	0.2716	−202	0.0866
818	−9	0.6317	−9	0.6326
768	−33	0.2012	−35	0.1697
671	−28	0.6388	−45	0.6165
666	97	0.3668	47	0.3394
658	8	0.7380	7	0.7325
645	−124	0.4405	−120	0.0433
532	−9	0.6141	−11	0.6129
392	−140	0.3830	−139	-0.0579
389	−14	0.3456	−47	0.3436
329	237	0.4629	228	0.2116
294	−370	0.5035	−44	0.3314
190	−370	0.5748	−370	0.4096
110	−36	0.4833	−69	0.4289
100	−9	0.3999	−14	0.4101
89	249	0.3665	247	0.1025
69	246	0.3547	244	−0.0086
20	−108	0.1720	36	0.1041

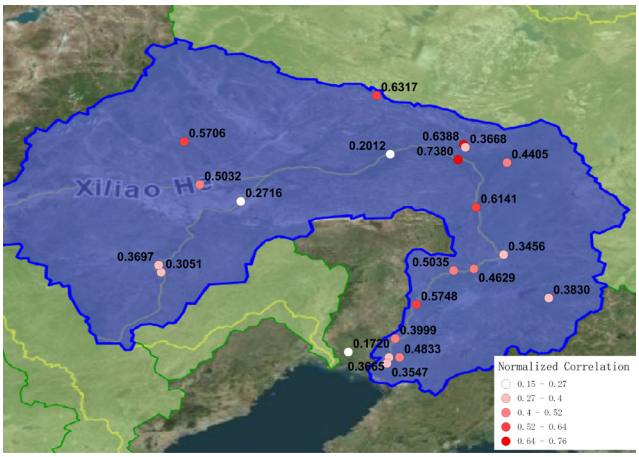

Fig. 3 Normalized correlation of reliable stations in the Liao River basin

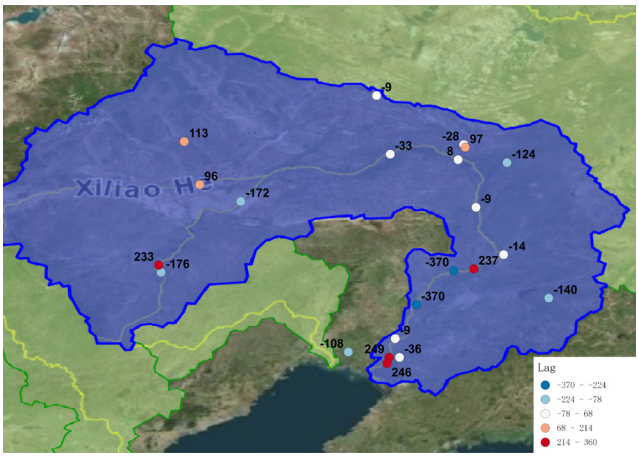

Fig. 4 Phase lags of reliable stations in the Liao River basin

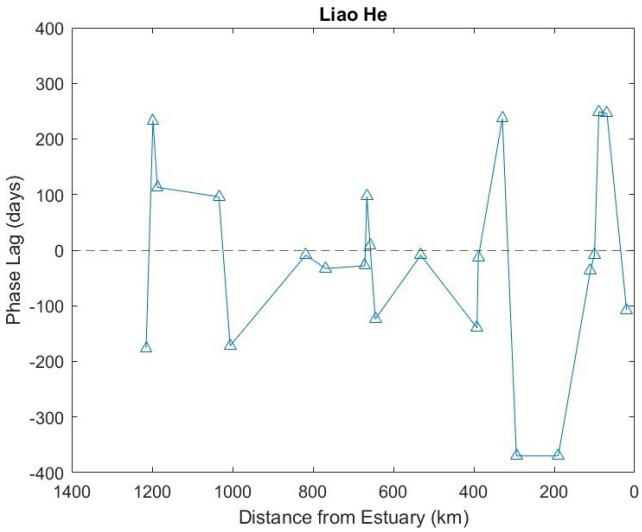

Fig. 5 Phase lags change by distance (in kilometers) from the estuary

in the table header). The spatial distributions of correlation and phase lags are presented in Figs. 6 and 7, while Fig. 8 shows the phase lag variation by distance from the estuary.

Table 3 Results for reliable stations in Huai River basin

Reference distance (km)	Lag (days)	Normalized correlation	Loess lag (days)	Loess correlation
1225	−35	0.3342	−52	0.2892
1151	−98	0.5479	−82	0.5425
1040	−156	0.5646	−370	0.4079
1032	−209	0.6017	−227	0.2868
591	−13	0.6211	10	0.6348
478	45	0.4285	41	−0.0645
444	−18	0.4413	−48	0.4502
321	−2	0.6756	−37	0.6766

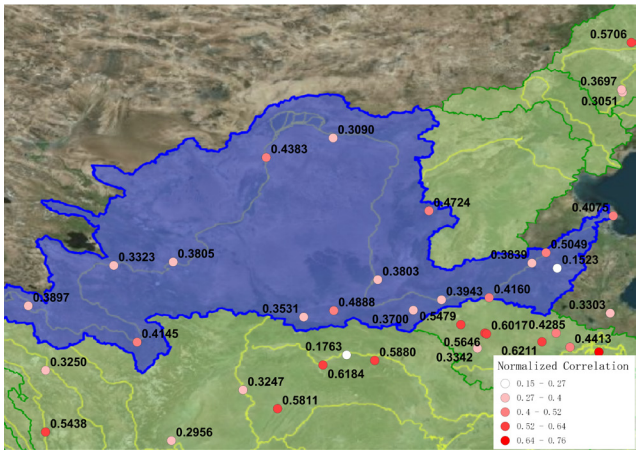

Fig. 6 Normalized correlation of reliable stations in the Huai River basin

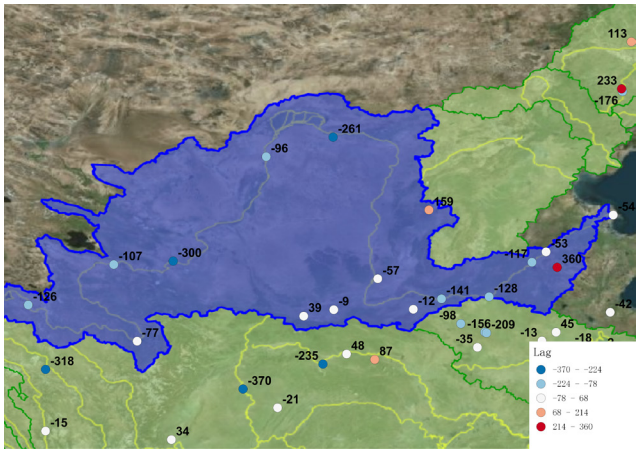

Fig. 7 Phase lags of reliable stations in the Huai River basin

5.3 Yellow River (Huang He)

The Yellow River, China's second-largest river, contains over 300 virtual stations. Among them, 45 were selected, evenly distributed along the river. The correlation of the full time series without phase shift ranges from −0.21 to 0.54. Results for reliable stations are listed in Table 4. Figs. 9 to 11 illustrate the spatial distribution of correlation and phase lags, and phase lag variation along the river, respectively.

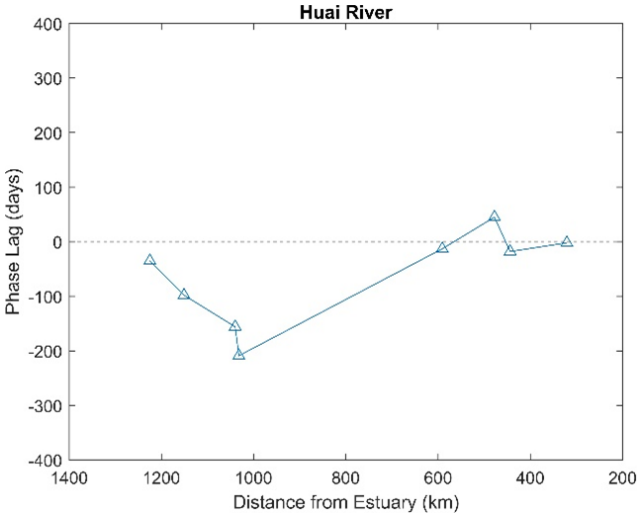

Fig. 8 Phase lags change by distance (in kilometers) from the estuary

Table 4 Results for reliable stations in the Yellow River basin

Reference distance (km)	Lag (days)	Normalized correlation	Loess lag (days)	Loess correlation
5230	−126	0.3725	−114	0.0701
4504	−77	0.4203	−75	0.1523
3802	−107	0.3332	−95	−0.0772
3473	−300	0.3742	−325	−0.0631
2652	−96	0.4476	−73	0.0585
2347	−261	0.3331	−275	−0.0080
1797	159	0.4968	166	−0.0066
1493	39	0.3558	54	0.3068
1374	−9	0.4929	−9	0.4947
1341	−57	0.3691	261	0.2384
1000	−12	0.3814	15	0.3704
881	−141	0.3937	−133	0.1367
687	−128	0.4231	−107	0.1208
513	360	0.1552	341	0.1822
412	−117	0.3960	−80	0.0732
336	−53	0.5050	9	0.4074
21	−54	0.4143	−65	0.2537

5.4 Yangtze River (Chang Jiang)

The Yangtze River, along with the Yellow River, is one of the most important rivers in China. It also has over than 300 virtual stations with water level data over the whole basin, however, unlike the Yellow River, which has numerous tributaries and a high-water volume, seasonal variations are also observed in both of GRACE water equivalent thickness and gauged water level dataset. The correlation of full time series without phase shift in Yangtze River basin falls between the range of 0.104 to 0.771. In the end, we summarize the results from all reliable stations in Table 5, show the spatial distribution in Figs. 12 and 13,

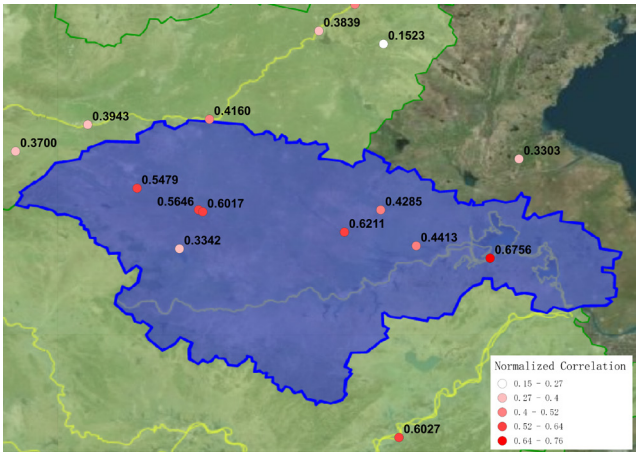

Fig. 9 Normalized correlation of reliable stations in the Yellow River basin

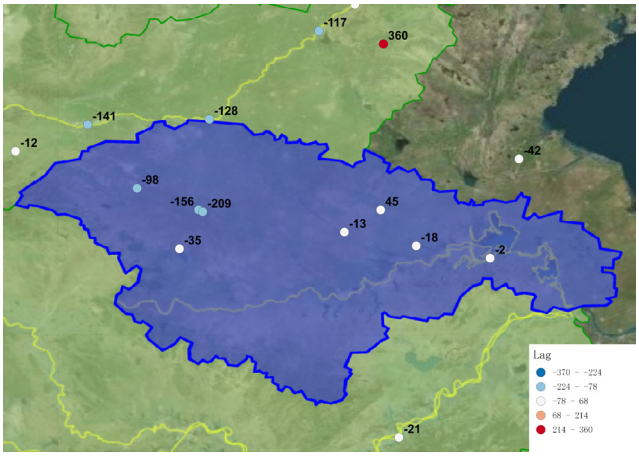

Fig. 10 Phase lags of reliable stations in the Yellow River basin

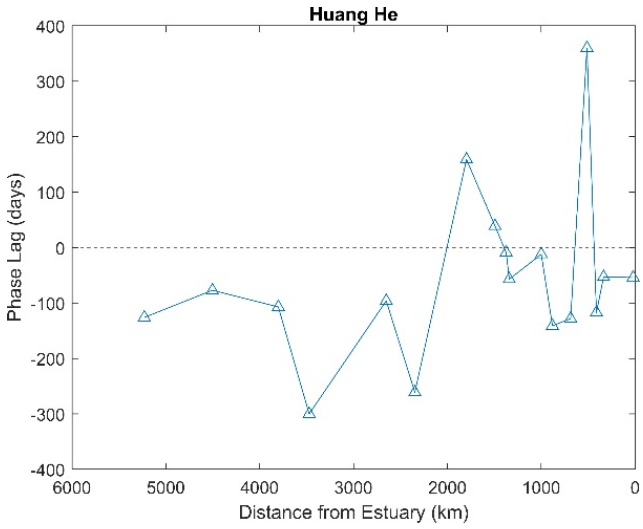

Fig. 11 Phase lags change by distance (in kilometers) from the estuary

and the change of the phase lag along the river on Fig. 14 as a function of the distance from the estuary in kms.

5.5 Pearl River (Zhu Jiang)

Seventeen virtual stations were selected from the Pearl River Basin. The correlation of the full time series without phase

Table 5 Results for reliable stations in the Yellow River basin

Reference distance (km)	Lag (days)	Normalized correlation	Loess lag (days)	Loess correlation
5622	−138	0.3497	−157	−0.3224
4480	−318	0.3250	14	0.2480
4336	−15	0.5438	3	0.5448
3424	−300	0.5392	−300	0.0273
2853	−358	0.5140	−324	0.2708
2771	34	0.2956	30	0.2125
2668	3	0.4524	9	0.4399
2560	−21	0.5811	−32	0.5696
2407	−4	0.7138	7	0.7226
2006	−189	0.5128	−201	0.0263
1901	−235	0.6184	−239	−0.3216
1775	−1	0.3716	−9	0.3732
1770	48	0.1763	−9	0.0725
1646	87	0.5880	81	0.3293
1641	11	0.4776	23	0.4482
1539	287	0.3615	282	−0.1249
1274	−27	0.7602	−39	0.7301
857	10	0.5315	39	0.4829
855	−98	0.4216	56	0.0504
788	−70	0.5715	−69	0.4151
474	−21	0.6027	151	0.5948

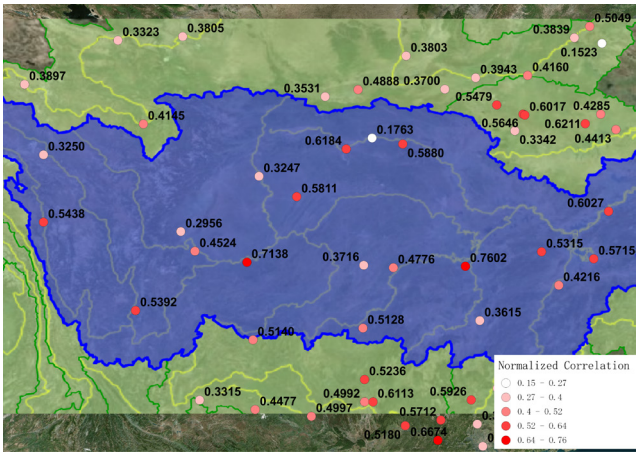

Fig. 12 Normalized correlation of reliable stations in the Yangtze River basin

shift ranges from 0.18 to 0.67. Table 6 presents the results for reliable stations, and Figs. 15 to 17 display the correlation, phase lags, and phase lag variation by distance, respectively.

6 Discussions

6.1 Attempt to determine correlation and phase lag

The GRACE time series represents the integrated water mass variation in whole river basins, while the gauged time series represents the locally water level variation. The correlations

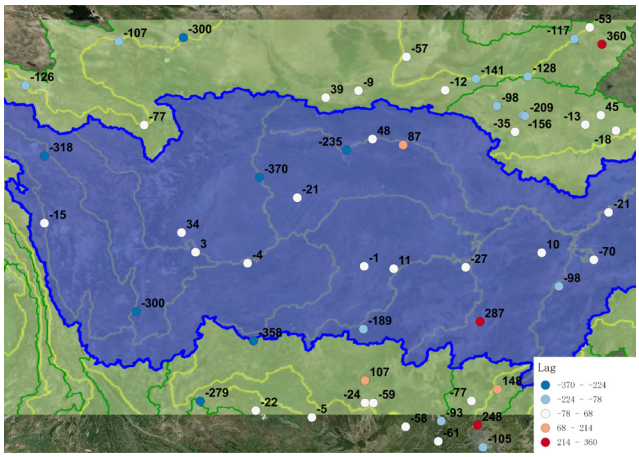

Fig. 13 Phase lags of reliable stations in the Yangtze River basin

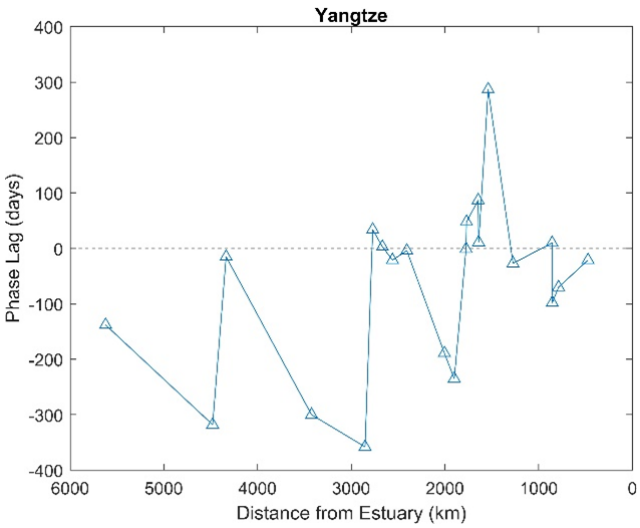

Fig. 14 Phase lags change by distance (in kilometers) from the estuary

Table 6 Results for reliable stations in the Pearl River basin

Reference distance (km)	Lag (days)	Normalized correlation	Loess lag (days)	Loess correlation
1618	−279	0.3315	69	0.0973
1380	−22	0.4477	−41	0.4316
1137	271	0.3482	54	0.1605
956	−5	0.4997	−9	0.511
928	107	0.5236	115	0.1756
891	−24	0.4992	−47	0.4655
730	−59	0.6113	−81	0.3296
425	−58	0.518	−72	0.3192
413	−93	0.5712	−89	0.2684
371	148	0.2813	58	0.127
339	−77	0.5926	−67	0.4359
249	−61	0.6674	−68	0.4882
174	248	0.3864	307	0.2869
75	−105	0.2917	−83	0.2831
69	27	0.4573	39	0.3773

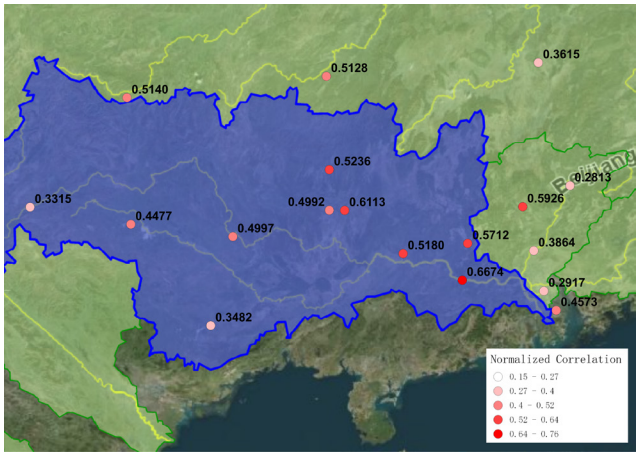

Fig. 15 Normalized correlation of reliable stations in the Pearl River basin

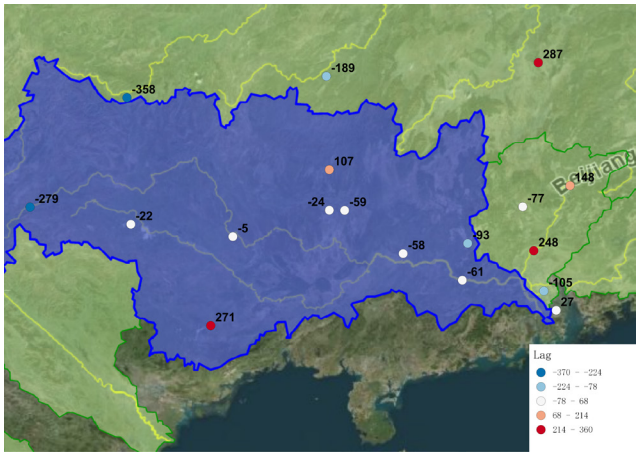

Fig. 16 Phase lags of reliable stations in the Pearl River basin

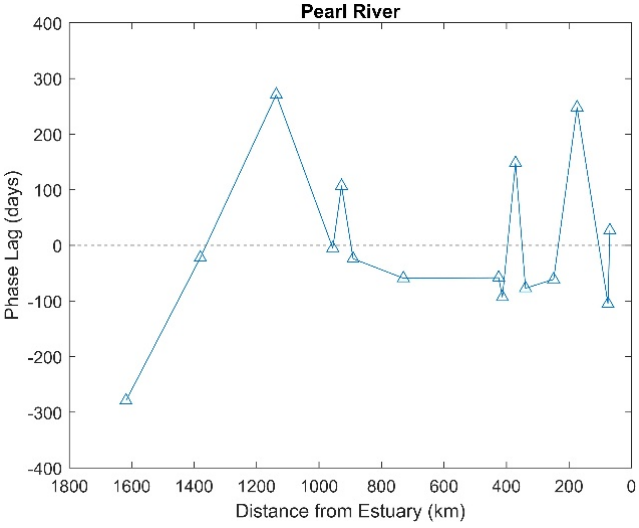

Fig. 17 Phase lags change by distance (in kilometers) from the estuary

of two dataset have some common features in all 5 basins. Usually, high local correlations of one basin are in the mainstream rather than on tributaries of the river, there will not be a high correlation at the source of the river. Based on the results available in this research, locally high correlations can concentrate in one section inside the river basin, but no overall trend as approaching to the estuary.

As for the phenomenon that high correlations can concentrates in one segment of river, in different basins these segments are not in the same position of the river. In the Liao and Yellow River basins, the area has more numbers of locally high correlations ap-pears in the central and upper part of the river, and in other basins, the position of this area is more advanced. It is worth noting that two high correlation stations of the Yangtze River occur exactly at the confluence of tributaries. Overall, the correlation between local water mass and average water mass variation does increase as the water moves away from river source, but there is no absolute increment.

Similar with the conclusion of correlation case, there is no clearly identified overall trends of phase lags along a river while approaching to the estuary. If we plot the phase lag as function of reference distance, the result is more intuitively that the value of phase lag fluctuates along the river basin (c.f., Figs. 5, 8, 11, 14 and 17). Expect for Liao River basin, other 4 river basins' phase lag value falls around 0 at the estuary.

The non-regular spatial distribution of the high correlation stations is assumed to be a mere coincidence. The reason why it is concentrated often to the central part of the basin is probably due to the higher probability of being more representative there than at the boundaries of the basins.

The optimal phase lag estimates along the longitudinal section of the river (see Fig. A3 in Appendix A as an example) might also be quite irregular, so no such a tendency could have been observed than in the case of the La Plata River basin [9]. Thus, the preconception that the water mass variation along a river occurs with a time delay as approaching to the estuary was not approved. It may indicate the consequence of the intense water management on most rivers of China. According to Dong et al. [29], the number of artificial reservoirs in China are exceeding 3500, and concentrated to the most populated regions of the country (see their Fig. 1). The very intense water management changes relevantly the subsurface water storage as well, which disarrays the GRACE-borne mass variation signal. All in all, the consequences of anthropogenic interferences are rather detected than natural variations of water mass.

6.2 Comparison with CLHMS for the period of 2003–2010

The reason behind irregular correlations and phase lags between average mass variation (observed by GRACE satellites) and gauged water level (hydrological stations),

probably is due to the impact of artificial hydrological management. China experiences rapidly growing water demands for the past decades and currently withdraws over 600 km^3 water annually from rivers, aquifers, reservoirs, etc. [29]. As Dong et al. [29] observed the consequences of the very intense water management in China; in order to validate the GRACE data, we choose a hydrologic model for these basins as a proper reference. The Coupled Land Surface Hydrologic Model System (CLHMS) of Dong et al. [29] is based on 30-year simulation to quantify the seasonal dynamics of China's reservoir water storage. The model coupling a total of 3,547 reservoirs, over the mainland China, which account for over 90% of the combined capacity for China's reservoirs. The simulated TWSA considering human water consumption and water management for 4 of the major river basins generated from the model was kindly provided to us by the authors.

The comparison result with GRACE mass variation in our research is in Fig. 18, confirmed that the correlation will be substantial increase if the impact of artificial water management is added in to hydrologic water level data. In addition, all 4 basins show significant overall correlation, comparing the results we obtained in Section 4 (Table 7).

Even though the CLHMS is not observed data but a complex model, it has been efficiently validated to other independent source by Dong et al. [29], thus by reason it was chosen to serve as the reference for the validation of GRACE EWH series. Therefore, we can conclude that the GRACE EWH time series contains dominant contribution from water mass variations and other sources are only in small extent these are influencing them.

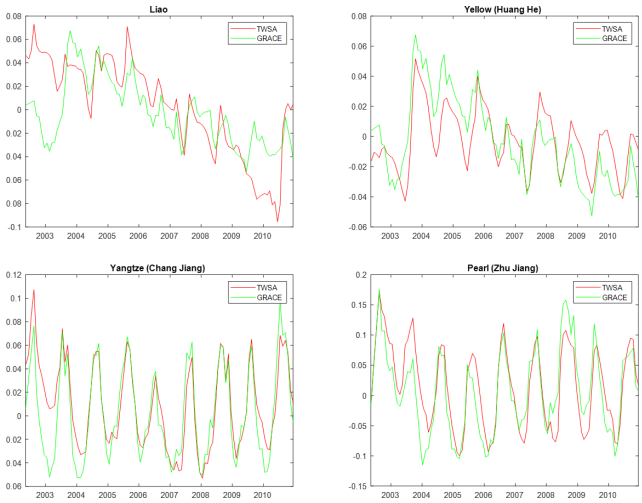

Fig. 18 Comparison of GRACE mass variation and simulated TWSA considering human water management for Liao, Yellow, Yangtze and Pearl River basins during 2003 and 2010

Table 7 Correlations of simulated TWSA and GRACE mass variation

Basins	Correlation
Liao River	0.6762
Yellow River	0.7811
Yangtze River	0.8439
Pearl River	0.8187

6.3 Comparison with ERA5-Land for the period of 2002–2023

The results then have been compared to water storage estimates for the test basins in the ERA5-Land model [30]. The ERA5-Land is a climate reanalysis, based on the land component of the ERA5 model forced by meteorological fields from ERA5, run at an enhanced spatial resolution (9 km *vs*. 31 km in ERA5) and an hourly temporal resolution. The ERA5-Land is using the Tiled ECMWF Scheme for Surface Exchanges over Land incorporating land surface hydrology (H-TESSEL). It uses version CY45R1 of the ECMWF's Integrated Forecasting System (IFS).

The water storage (*WS*) is estimated basin-wise, by determining from ERA5-Land the precipitation (*PT*) evapotranspiration (*ET*), and runoff (*RO*) [31], then.

$$WS = PT - ET - RO. \tag{8}$$

As water storage contributes a massive mass anomaly on long time scales as well, it is expected to be observed by GRACE and GRACE-FO monthly solutions.

Fig. 19 displays the linear trend of the ERA5-Land water storage signal determined by Eq. (8) and subsequently Eq. (7), and Fig. 20 the linear trends of surface mass anomaly from GRACE and GRACE-FO models determined by Eqs. (1) and (7).

Although there are obvious similarities of the spatial distribution of the mass change, the difference of the power

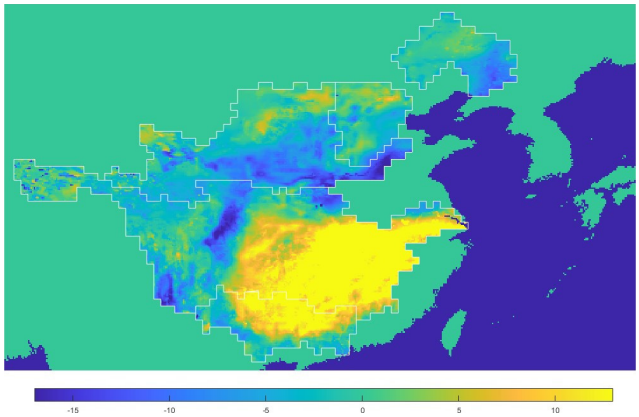

Fig. 19 Linear trend of water storage variations for the period of 2002–2023 based on ERA5-Land reanalysis (unit: mm/year)

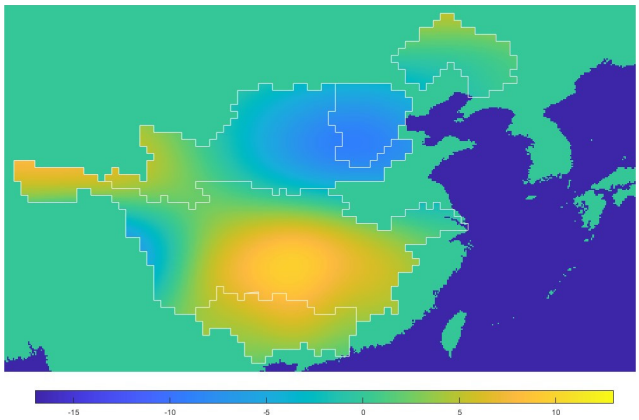

Fig. 20 Linear trend of surface mass anomaly for the period of 2002–2023 based on GRACE and GRACE-FO JPL monthly solutions (unit: mm/year)

of the signal is dominant. As GRACE monthly solutions have been smoothed by a Gaussian filter with a radius of 300 km in order to eliminate the so-called striping error, the same filter was applied to linear trends derived from ERA5-Land (Fig. 19) and resulted in Fig. 21.

When comparing Figs. 20 and 21, the water storage can be identified as the major contribution of the surface mass anomaly (c.f., the same color scale on the figures). The 2D-correlation of the ERA5-Land trends and of the GRACE/GRACE-FO trends have been determined and summarized in Table 8.

In the case of Liao River, there was no correlation observed. Furthermore, the western parts of the Yangtze and Yellow River Basins became influenced by some mass

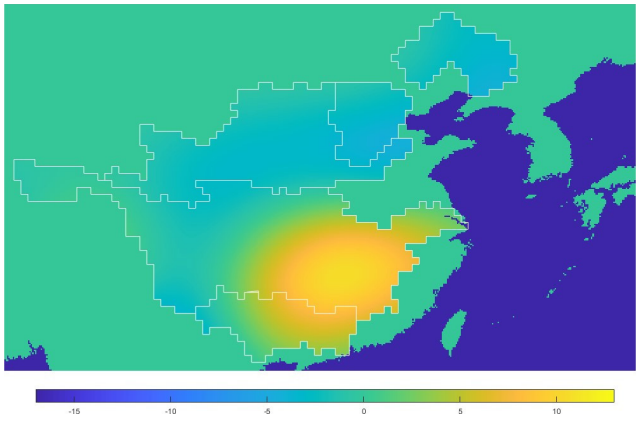

Fig. 21 Linear trend of water storage variations smoothed by a 2D-Gaussian filter with 300 km radius for the period of 2002–2023 based on ERA5-Land reanalysis (unit: mm/year)

Table 8 2D-Correlations of ERA5-Land and GRACE mass variations

Basins	2D-correlation of GRACE and ERA5-Land	2D-correlation of GRACE and smoothed ERA5-Land
Liao River	−0.1020	−0.3717
Huai He	0.9190	0.6770
Yellow River	0.4850	0.6515
Yangtze River	0.5792	0.7328
Pearl River	0.7359	0.8271
All basins	0.5818	0.6856

change from outside of the test area. However, the rest of the basins shows convincing correlation with the GRACE data with similar magnitude of the mass content change.

7 Conclusions

The presumption of observing a phase lag between local *in situ* tide gauge observations and integrated mass changes from GRACE-borne surface mass anomaly time series – an effect observed in the La Plata River basin [9] – could not be established in any of the major river basins in China. This may indicate the influence of intensive water management practices prevalent across most of China's rivers. This finding aligns with Kiss and Földváry [9], who concluded that no periodicity in water mass variations was observed for rivers under heavy water control, whether using GRACE data or tide gauge water levels. The intense water management in China significantly alters subsurface water storage, which disrupts the GRACE-derived mass variation signal. Consequently, anthropogenic influences dominate the observed mass variations rather than natural fluctuations in water mass.

Despite this outcome, the GRACE-derived surface mass variations were validated by comparing them with the temporal variations of the simulated total water storage anomaly from the CLHMS hydrological model [29], and with the spatial variations from the ERA5-Land model [30].

Acknowledgement

The project presented in this article is supported by the Ministry of Culture and Innovation through the National Research, Development and Innovation Fund, project ID 2022-2.1.1-NL-2022-00012 National Laboratory of Cooperative Technologies.

References

[1] Smylie, D. E. "Earth Dynamics: Deformations and Oscillations of the Rotating Earth", Cambridge University Press, 2013. ISBN 978-0-521-87503-5

[2] National Research Council "Satellite Gravity and the Geosphere: Contributions to the Study of the Solid Earth and Its Fluid Envelopes", The National Academies Press, 1997. ISBN 0-309-05792-2 https://doi.org/10.17226/5767

[3] Bettadpur, S. V., Tapley, B. D. "Accuracy Assessments of Dedicated Geopotential Mapping Missions", Supplement to EOS, Transactions of the American Geophysical Union, 77(46), F140, 1996.

[4] Földváry, L., Abdelmohsen, K., Ambrus, B. "Water Density Variations of the Aral Sea from GRACE and GRACE-FO Monthly Solutions", Water, 15(9), 1725, 2023. https://doi.org/10.3390/w15091725

[5] Reigber, C., Schwintzer, P., Lühr, H. "The CHAMP Geopotential Mission", Bollettino di Geofisica Teoretica ed Applicata, 40(3–4), pp. 285–289, 1999. [online] Available at: https://bgo.ogs.it/sites/default/files/2023-08/bgta40.3.4_REIGBER1.pdf [Accessed: 07 November 2025]

[6] Jekeli, C. "The determination of gravitational potential differences from satellite-to-satellite tracking", Celestial Mechanics and Dynamical Astronomy, 75(2), pp. 85–101, 1999. https://doi.org/10.1023/A:1008313405488

[7] Visser, P. N., Rummel, R., Balmino, G., Sünkel, H., Aguirre, M., Woodworth, P. L., Tscherning, C. C., Sabadini, R. "The European Earth Explorer Mission GOCE: Impact for the Geosciences", In: Mitrovica, J. X., Vermeersen, B. L. A. (eds.) Ice Sheets, Sea Level and the Dynamic Earth (Geodynamics Series), American Geophysical Union, 2002, pp. 95–107. ISBN 9780875905310 https://doi.org/10.1029/GD029p0095

[8] Ilk, K. H., Flury, J., Rummel, R., Schwintzer, P., Bosch, W., …, Gruber, T. "Mass Transport and Mass Distribution in the Earth System: Contribution of the New Generation of Satellite Gravity and Altimetry Missions to Geosciences", [pdf] GeoForschungsZentrum, Potsdam, Germany, 2005. Available at: https://mediatum.ub.tum.de/doc/1367829/document.pdf [Accessed: 07 November 2025]

[9] Kiss, A., Földváry, L. "Comparison of Seasonal Hydrologic Variations in the La Plata Basin from GRACE Monthly Solutions with In situ Tide Gauge Water Level Data", Acta Geodynamica et Geomaterialia, 14(2), pp. 145–152, 2017. https://doi.org/10.13168/AGG.2016.0035

[10] Li, W., Wang, K., Li, X. "Spatial and temporal analysis of daily terrestrial water storage anomalies in China", Acta Geodaetica et Geophysica, 59(4), pp. 427–440, 2024. https://doi.org/10.1007/s40328-024-00452-z

[11] Li, X., Li, W. "利用ITSG-Grace2018天解时变模型探测短时洪涝" (Using ITSG-Grace2018 daily solutions time-varying model to detect short-term flood), Journal of Geodesy and Geodynamics, 43(4), pp. 414–419, 2023. (in Chinese) https://doi.org/10.14075/j.jgg.2023.04.015

[12] Földváry, L., Aminjanova, M. "Evaluation of the impact of the biomass on GRACE-borne total water storage estimates in the Amazon Basin", Geodesy and Geodynamics, in press. (Accepted for publication: February 2026) https://doi.org/10.1016/j.geog.2025.12.005

[13] Földváry, L. "Desmoothing of averaged periodical signals for geodetic applications", Geophysical Journal International, 201(3), pp. 1235–1250, 2015. https://doi.org/10.1093/gji/ggv092

[14] Xiao, C., Zhong, Y., Feng, W., Gao, W., Wang, Z., Zhong, M., Ji, B. "Monitoring the Catastrophic Flood With GRACE-FO and Near-Real-Time Precipitation Data in Northern Henan Province of China in July 2021", IEEE Journal of Selected Topics in Applied Earth Observations and Remote Sensing, 16, pp. 89–101, 2023. https://doi.org/10.1109/JSTARS.2022.3223790

[15] Zhang, X., Wang, X., Török, Z. G. "A városi zöldfelületek szerepe az árvízveszély csökkentésében: A kínai Zhengzhou Erqi kerületének GIS-modellezési esettanulmánya" (The role of urban green spaces in flood hazard reduction: A GIS modeling case study of the Erqi District of Zhengzhou, China), Geodézia és Kartográfia, 76(3–4), pp. 4–11, 2024. (in Hungarian) https://doi.org/10.30921/GK.76.2024.3-4.1

[16] Zhou, H., Luo, Z., Tangdamrongsub, N., Wang, L., He, L., Xu, C., Li, Q. "Characterizing Drought and Flood Events over the Yangtze River Basin Using the HUST-Grace2016 Solution and Ancillary Data", Remote Sensing, 9(11), 1100, 2017. https://doi.org/10.3390/rs9111100

[17] Swenson, S., Wahr, J. "Methods for inferring regional surface-mass anomalies from Gravity Recovery and Climate Experiment (GRACE) measurements of time-variable gravity", Journal of Geophysical Research, 107(B9), pp. ETG 3-1–ETG 3-13, 2002. https://doi.org/10.1029/2001JB000576

[18] Swenson, S., Wahr, J. "Post-processing removal of correlated errors in GRACE data", Geophysical Research Letters, 33(8), L08402, 2006. https://doi.org/10.1029/2005GL025285

[19] Bettadpur, S. "Gravity Recovery and Climate Experiment: Level-2 Gravity Field Product User Handbook", Center for Space Research, The University of Texas at Austin, Austin, TX, USA, CSR-GR-03-01, 2018. [online] Available at: https://archive.podaac.earthdata.nasa.gov/podaac-ops-cumulus-docs/grace/open/docs/L2-UserHandbook_v4.0.pdf [Accessed: 07 November 2025]

[20] Dahle, C., Flechtner, F., Murböck, M., Michalak, G., Neumayer, H., Abrykosov, O., Reinhold, A., König, R. "GRACE Geopotential GSM Coefficients GFZ RL06, V. 6.0", GFZ Data Services, Potsdam, Germany, 2018. https://doi.org/10.5880/GFZ.GRACE_06_GSM

[21] Longuevergne, L., Scanlon, B. R., Wilson, C. R. "GRACE Hydrological estimates for small basins: Evaluating processing approaches on the High Plains Aquifer, USA", Water Resources Research, 46(11), W11517, 2010. https://doi.org/10.1029/2009WR008564

[22] NASA "GRACE(-FO) Data Analysis Tool, (RL06.3)", [computer program] Available at: https://grace.jpl.nasa.gov/data/data-analysis-tool/ [Accessed: 07 November 2025]

[23] Crétaux, J.-F., Arsen, A., Calmant, S., Kouraev, A., Vuglinski, V., …, Maisongrande, P. "SOLS: A lake database to monitor in the Near Real Time water level and storage variations from remote sensing data", Advances in Space Research, 47(9), pp. 1497–1507, 2011. https://doi.org/10.1016/j.asr.2011.01.004

[24] NIST/SEMATECH "e-Handbook of Statistical Methods", NIST/SEMATECH, Gaithersburg, MD, USA, 2012. https://doi.org/10.18434/M32189

[25] Cleveland, W. S. "Robust Locally Weighted Regression and Smoothing Scatterplots", Journal of the American Statistical Association, 74(368), pp. 829–836, 1979. https://doi.org/10.1080/01621459.1979.10481038

[26] Cleveland, W. S., Devlin, S. J. "Locally Weighted Regression: An Approach to Regression Analysis by Local Fitting", Journal of the American Statistical Association, 83(403), pp. 596–610, 1988. https://doi.org/10.1080/01621459.1988.10478639

[27] Rabiner, L. R., Gold, B. "Theory and Application of Digital Signal Processing", Prentice-Hall, 1975. ISBN 0139141014

[28] Kajári, B., van Leeuwen, B. "Sentinel-1 és Sentinel-2 felvételek belvíz-veszélyeztetettségi idősoros elemzése konvolúciós neurális hálózatokkal" (Time Series Analysis of Flood Risk Using Sentinel-1 and Sentinel-2 Images with Convolutional Neural Networks), Geodézia és Kartográfia, 76(1), pp. 10–16, 2024. (in Hungarian) https://doi.org/10.30921/GK.76.2024.1.2

[29] Dong, N., Wei, J., Yang, M., Yan, D., Yang, C., …, Yu, Z. "Model Estimates of China's Terrestrial Water Storage Variation Due To Reservoir Operation", Water Resources Research, 58(6), e2021WR031787, 2022. https://doi.org/10.1029/2021WR031787

[30] Muñoz-Sabater, J., Dutra, E., Agustí-Panareda, A., Albergel, C., Arduini, G., …, Thépaut, J.-N. "ERA5-Land: a state-of-the-art global reanalysis dataset for land applications", Earth System Science Data, 13(9), pp. 4349–4383, 2021. https://doi.org/10.5194/essd-13-4349-2021

[31] Trajkovic, S., Gocic, M. "Temperature-based Evapotranspiration in the WSVI Drought Index Implementation: Case Study: Pannonian Basin", Periodica Polytechnica Civil Engineering, 68(3), pp. 774–780, 2024. https://doi.org/10.3311/PPci.23734

Appendix A

By plotting the time series for each station, we can visually inspect the fluctuations and trends of the curves, providing an intuitive interpretation of the correlation results. Below are some examples from the Liao River, where visual inspection often overrides the statistical outcomes.

For instance, Station KM1074 in the Liao River Basin shows a normalized correlation coefficient of 0.26. Comparing the gauged water level with the GRACE water equivalent thickness reveals that the two time series do not align well during the first half of the period (Fig. A1). This discrepancy is particularly evident when applying the Loess method (see red and green curves in Fig. A1). Fig. A2 presents the results after shifting one of the curves by the phase corresponding to the maximum cross-correlation value.

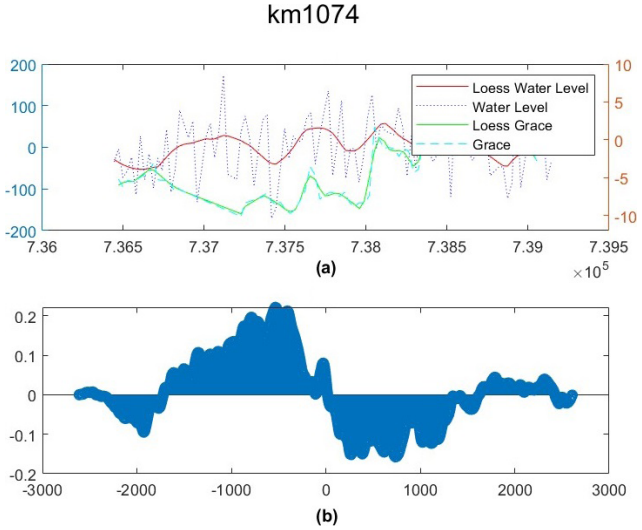

Fig. A1 Comparison of gauged water level at KM 1074 section of the Liao River *vs*. GRACE-borne surface mass data for the whole Liao River basin: (a) time series; (b) estimated cross correlation of the two time series

In the cases of station KM1074, the correlation of 0.26 is so small, the we have to conclude that locally the impact of the hydrological processes is not dominant among other mass redistribution processes, therefore the interpretation of the observed mass variation signal for hydrological mass variations would be incorrect. Accordingly, most stations with correlation value less than 0.3 were excluded, not considered to be reliable stations. Only in a few cases it was decided to be worth for discussing. For example, correlation of KM0020 is 0.2007 (< 0.3), but by visual check we can observe relevant tendency of the two signals (Fig. A3), but due to the effect of some other mass varying processes, the similarity statistically cannot be detected (Fig. A4). The periodicity of the signals

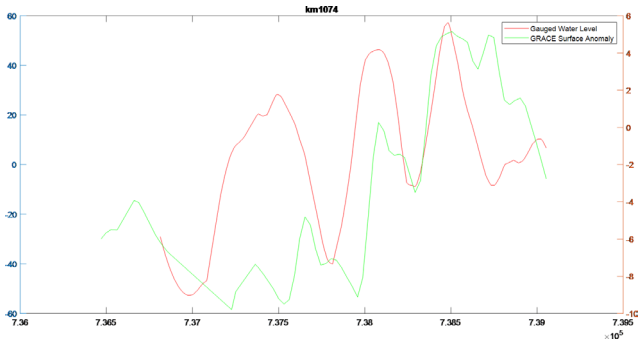

Fig. A2 The two data sets of Fig. A1 shifted by the phase lag of the best cross-correlation values

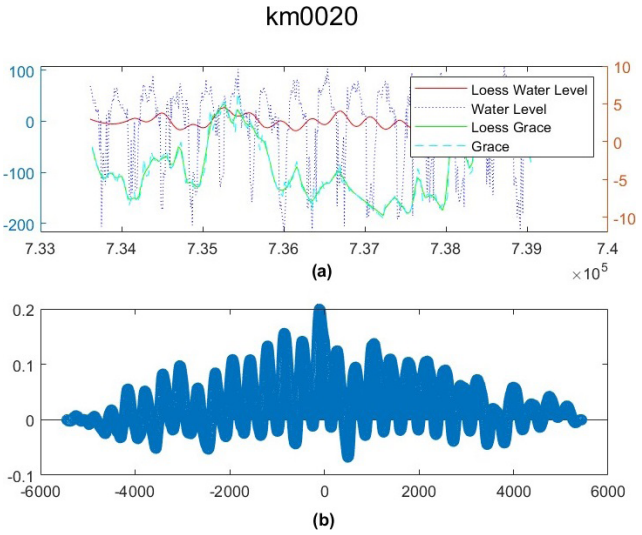

Fig. A3 Comparison of gauged water level at KM 0020 section of the Liao River *vs*. GRACE-borne surface mass data for the whole Liao River basin: (a) time series; (b) estimated cross correlation of the two time series

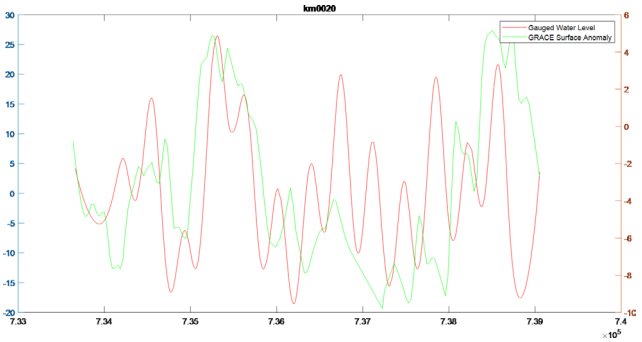

Fig. A4 The two data sets of Fig. A3 shifted by the phase lag of the best cross-correlation values

is similar, (particularly when Loess method is applied), so reliable estimation of the phase can be expected. The correlation coefficient is small due to the impact of some other mass variation signal occurring with notably longer periodicity, so this station can be included in the test.

Station KM0020 also has a longer time series compared to most stations in the Liao River basin (starting in 2008, while others began in 2016), which likely contributes to a lower correlation over a longer data span. For comparison, station KM0984 had a higher correlation coefficient of 0.6272. However, visual inspection (Figs. A5 and A6) shows that the two time series do not align well at the best correlation position. This discrepancy arises due to the short duration of the time series (from October 2020 to the present). Shorter time series tend to produce simpler curves with fewer fluctuations, resulting in artificially high correlation values without indicating real consistency between the two time series.

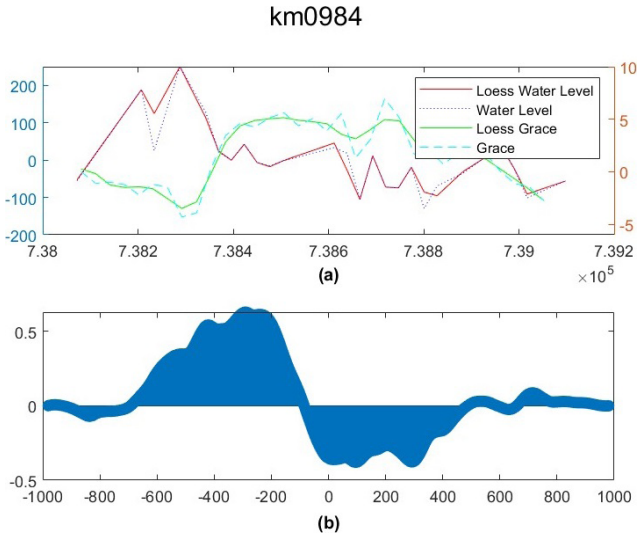

Fig. A5 Comparison of gauged water level at KM 0984 section of the Liao River *vs*. GRACE-borne surface mass data for the whole Liao River basin: (a) time series; (b) estimated cross correlation of the two time series

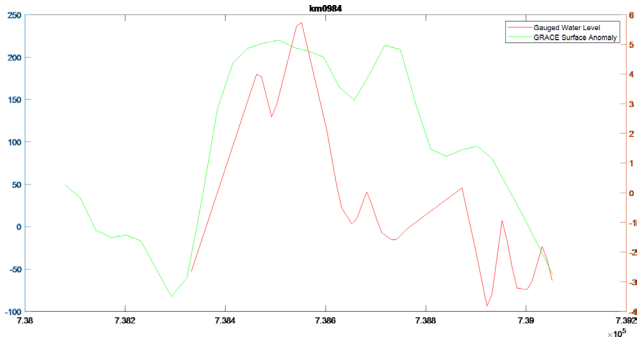

Fig. A6 The two data sets of Fig. A5 shifted by the phase lag of the best cross-correlation values